APL Materials

Effect of electron conduction on the read noise characteristics in ReRAM devices

Cite as: APL Mater. **10**, 101114 (2022); https://doi.org/10.1063/5.0109787
Submitted: 14 July 2022 • Accepted: 28 September 2022 • Published Online: 31 October 2022

K. Schnieders, C. Funck, F. Cüppers, et al.

AIP Publishing

Effect of electron conduction on the read noise characteristics in ReRAM devices

Cite as: APL Mater. 10, 101114 (2022); doi: 10.1063/5.0109787
Submitted: 14 July 2022 • Accepted: 28 September 2022 •
Published Online: 31 October 2022

K. Schnieders,[1,2,a] C. Funck,[1] F. Cüppers,[2,3] S. Aussen,[1,2] T. Kempen,[2,3] A. Sarantopoulos,[1] R. Dittmann,[1] S. Menzel,[1] V. Rana,[3] S. Hoffmann-Eifert,[3] and S. Wiefels[1]

AFFILIATIONS

[1] Peter Grünberg Institute 7, Forschungszentrum Jülich GmbH and JARA-FIT, Wilhelm Johnen Str., 52428 Jülich, Germany
[2] RWTH Aachen University, Templergraben 55, 52062 Aachen, Germany
[3] JARA-Institute Green IT, Forschungszentrum Jülich GmbH, Wilhelm Johnen Str., 52428 Jülich, Germany

[a] **Author to whom correspondence should be addressed**: k.schnieders@fz-juelich.de

ABSTRACT

The read variability of redox based resistive random access memory is one of the key characteristics with regard to its application in both data storage and novel computation in memory or neuromorphic architectures. While intrinsic noise limits the number of distinguishable states, it may be beneficial for probabilistic computing or to prevent overfitting. Thus, application and material system need to be carefully matched according to their read noise characteristics. Preceding density functional theory simulations suggested dividing oxides used in valence change memory into two categories based on the dominating conduction mechanism. We provide a comprehensive experimental study, which confirms the simulations and demonstrates how the conduction mechanism affects the variability. We analyze the signal-to-noise ratio (SNR) of five different switching oxides, revealing that oxides with shallow defect states (type 1) show high SNR whereas oxides with deep defect states (type 2) exhibit pronounced ionic noise. Thus, our results provide valuable input toward tuning of read noise characteristics by material design.

I. INTRODUCTION

One of the most investigated classes of resistive random access memory (RRAM) is redox based RRAM (ReRAM) devices. These are highly scalable,[1,2] two-terminal devices, which show high endurance up to more than 10^{10} switching events,[3–5] high retention,[6–8] and switching speeds substantially lower than 1 ns for many materials,[9,10] and comparatively simple design. Hence, ReRAM might play an important role in future storing and calculation applications.[11–13] Furthermore, many interesting logic and computation in memory schemes were developed that provide the chance to overcome the limitations of current processor architectures, such as the von Neumann bottleneck.[14–17] One of the widely investigated ReRAM classes is based on the valence change mechanism (VCM).[18,19] VCM-type ReRAM cells consist of a metal/metal oxide/metal stack with asymmetric metal electrodes of different work functions and Gibbs free energy of oxidation. The metal oxide can be realized as a single-layer[20,21] or bi-layer.[22,23] The operation principle of ReRAM is applying well-chosen voltage schemes to vary the concentration and distribution of oxygen vacancies at the active Schottky interface of the devices and by this tune the resistance of the device.

A major challenge for the reliability of ReRAM is the short term instability of the programmed states while reading, often called read noise.[24–26] This limits the reliability of stored information.[13] In particular, if a large number of logical states are used, read noise can cause undesired state transition. Even if only two states are defined, non-intended switching was observed.[27] In addition, if utilized for neuromorphic operations, even though a certain degree of stochasticity might be desired to prevent overfitting,[28–30] a reliable quantification of the phenomenon is of major importance.

Recent density functional theory (DFT) studies revealed the strong link between the position of the oxygen vacancy levels in the bandgap of the switching oxide layer, the resulting current transport mechanism, and the current–voltage (I–V) characteristic in VCM

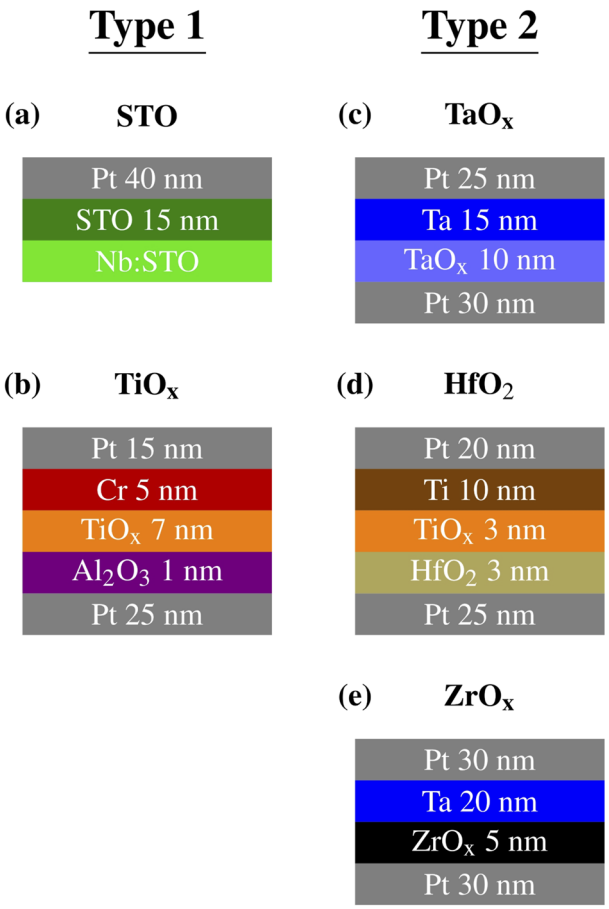

FIG. 1. The design of devices tested for this paper. In the course of this paper, we use the abbreviation above the stacks as a synonym for the device.

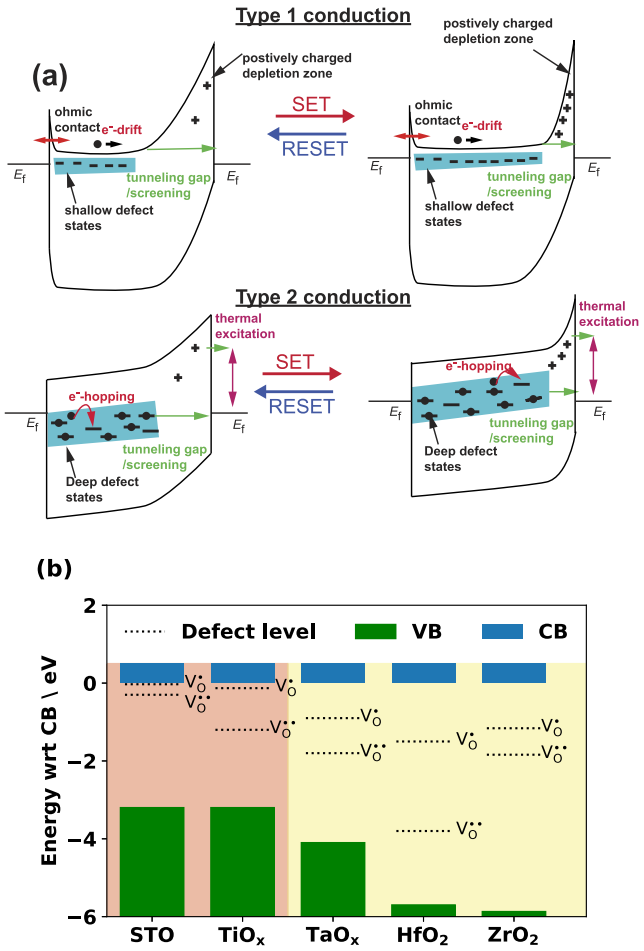

FIG. 2. (a): Illustration of the conduction types 1 and 2 taken from Funck and Menzel.[31] For type 1 materials, the main conduction mechanism inside the switching oxide is the excitation of electrons into the CB. The electrons cross the Schottky barrier by tunneling out of the CB. For type 2 materials, the electron is transferred by hopping between defect states. At the AE, the electrons tunnel from defect states into the bordering metal layer. Panel (a) was reproduced with permission from C. Funck and S. Menzel, "Comprehensive model of electron conduction in oxide-based memristive devices," ACS Appl. Electron. **3**, 3674–3692 (2021). Copyright 2021 ACS.[31] (b) The energy landscapes of the switching oxides measured are shown. In particular, the gap between the oxygen defect states and the CB is to be noted. The energy levels are plotted with reference to the lower edge of the CB. The energy levels were experimentally determined for STO,[44] for TiO_x,[45] for TaO_x,[46] for HfO_2,[47] and for ZrO_x.[48]

devices.[31] We provide an experimental verification by the analysis of five typical ReRAM device stacks, with two material composition belonging to type 1 and three designs that were attributed to type 2. These can be seen in Figs. 1(a)–1(e). Furthermore, we extend the study of Funck and Menzel[31] by analysis of the noise characteristics for the two types of ReRAM devices.

II. CONDUCTION MECHANISM

Two conduction mechanisms were identified based on the oxygen vacancies in the material. The oxygen vacancies differing in the energy gap between the conduction band (CB) and the energy levels of the oxygen defect states.[32] A schematic representation of these conduction types is shown in Fig. 2(a). If the gap between CB and oxygen defect state is small enough, a relevant portion of the electrons can be thermally excited into the CB.[33] Thus, the tunneling from the oxide CB through the Schottky depletion zone into the metal conduction band has the dominating role in conduction. Here, the exact location of the defects is of no major importance for the electron conduction. Thus, a random walk of these defects only has a minor impact on the resistance. This conduction is called type 1. If, otherwise, the gap is substantially larger, making excitation into the CB energetically unfavorable, the current limiting conduction mechanism is the hopping from defect states to the metal interface of the active electrode. Here, the hopping of defects directly affects the electronic conductance. In this case, the material is assigned to conduction type 2. In both cases, the electrons bridge the energy barrier at the active electrode by tunneling. The central difference is the quasi-continuous distribution of states in the CB, allowing for a high population of electrons near the tunneling barrier for type 1 materials, whereas for type 2

TABLE I. Experimental settings and dimensions of ReRAM devices.

	STO	TiO_x	TaO_x	HfO_2	ZrO_x
$\lvert V_{read}\rvert$ (V)	0.5	1	0.25	0.25	0.35
$\lvert V_{Set}\rvert$ (V)	2–2.5	2.0–2.3	0.9–1.5	1.2 to 1.2	1
$\lvert V_{Reset}\rvert$ (V)	2.2–2.5	2.0–2.3	1.3–1.7	1.0–1.5	1.8
$t_{rise,\,switch}$ (μs)	500	300	2	2	40
$t_{pulse,\,switch}$ (ms)	50–100	200–700	$1 \cdot 10^{-3}$	0.02	0
$t_{rise,\,read}$ (μs)	200	200	200	200	200
$t_{pulse,\,read}$ (s)	2	2	2	2	2
A_{device} (nm^2)	$4.8 \cdot 10^7$	$2.5 \cdot 10^5$	$4 \cdot 10^6$	$1 \cdot 10^4$	$4.9 \cdot 10^7$
d_{oxide} (nm)	15	7	10	3/3	5
$T_{on\text{-}off}$	2	2	5	5	5
References	50	51	3	49	39

oxides, a small number of defect states provide the tunneling state. This model is supported by theoretical and experimental findings alike.[20] Note that compared to type 1 materials, such as $SrTiO_3$ (STO),[34] the resistance of type 2 materials is less influenced by the temperature.[35] To further prove the model, we compare the expected and experimental variability of the two conduction types. If one of these defects changes its position, abrupt current jumps are expected, as observed, for example, in HfO_2[36,37] and Ta_2O_5/TaO_2[38] based devices. This type of noise was attributed to the migration of ions for ZrO_2.[39,40] This type of noise is often referred to as random telegraph noise (RTN). We will instead use the name ionic noise, as the term RTN is commonly used mostly for two-level noise in metal-oxide-semiconductor field-effect transistor devices,[41–43] because the mechanisms inducing this kind of noise are not exactly the same, and the noise we observed does not exactly match the expectations of RTN.

According to this study, five different VCM-type ReRAM devices are selected. The abbreviations, stack sequences and dimensions, as well as experimental settings for stable bipolar switching behavior, are summarized in Figs. 1(a)–1(e) and Table I. Here, the devices are refered to by their main switching metal oxide layer being STO, TiO_x, TaO_x, HfO_2, and ZrO_x. We decided to use well understood material stacks that will be subject to further research, even though some variations apart from the switching layer are present. Note that previous studies revealed that in the HfO_2 devices, the switching takes place in the HfO_2 and

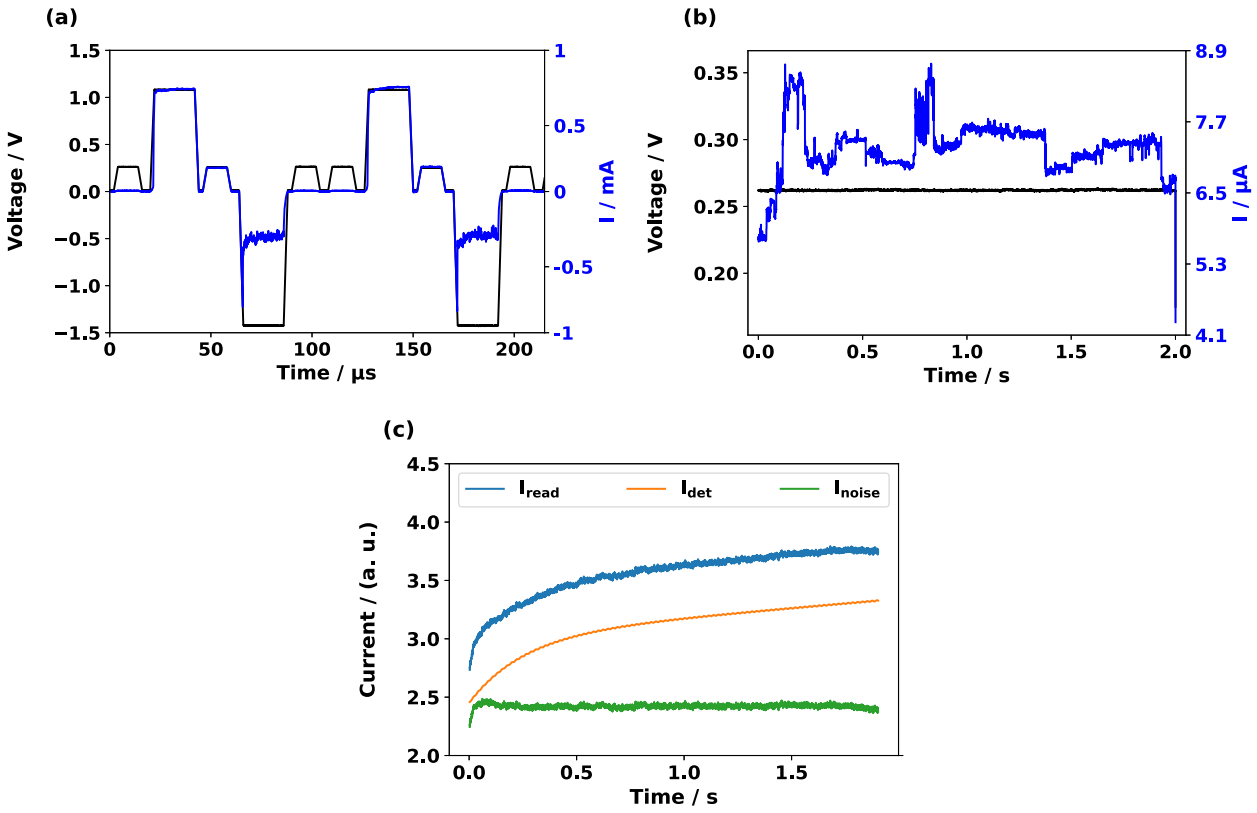

FIG. 3. Measurement routine used for recording the read noise. (a) Shows the switching pulses with subsequent reads, which are applied at least two times as seen from the black curve. (b) Refers to the constant read pulse that is applied for 2 s. In case the device is switched, the read signal is evaluated. In (a) and (b), the current response of a HfO_2 device is plotted exemplarily for switching and reading, respectively. The pre-processing of type 1 traces is shown in (c). The noise induced by the power grid and the deterministic part described by the trace Eq. (1) (orange line) is subtracted from the trace (blue line) to receive the noise signal (green line). An offset was added to the data to ease visually distinguishing the parts of the signal.

not in the TiO_x layer.[49] The TiO_x layer mainly functions as an internal resistor.

The relative positions of the oxygen vacancy states in the oxygen layers are shown in Fig. 2(b). Due to the energy level of the defect states, we assign the TiO_x and STO devices to conduction type 1,[20,33,34] because the energy difference between the CB and the nearest oxygen defect state V_O is shallow.[44,45] The other material systems are expected to belong to type 2.[46–48]

III. EXPERIMENTAL ROUTINE

For the measurement of the I–V sweeps, we used a Keithley 2611 source measure unit. We adapted the parameters of the voltage sweeps according to the experience with the particular material system. The read noise experiments were performed using the Keithley 4200-SCS measurement setup. The measurement routine consists of two waveforms. First, the device is switched at least two times, as seen in Fig. 3(a). By including read signals in the waveform, we verify that the device still switches reliably. Subsequently, we read the device for 2 s at a constant read voltage. We call the current response of this read pulse a trace. This is exemplarily shown in Fig. 3(b). The experimental parameters are listed in Table I. The parameters were adjusted for each device to ensure stable switching over time for different devices. After the switching sequence, the devices were in the high resistive state (HRS). We decided to focus on the HRS, as here the read noise is more noticeable.

A trace was taken into account if the relative resistive change in the previous switching cycles exceeded a threshold $T_{\text{on-off}}$. This threshold was individually chosen for every material system, based on its commonly observed switching characteristics.

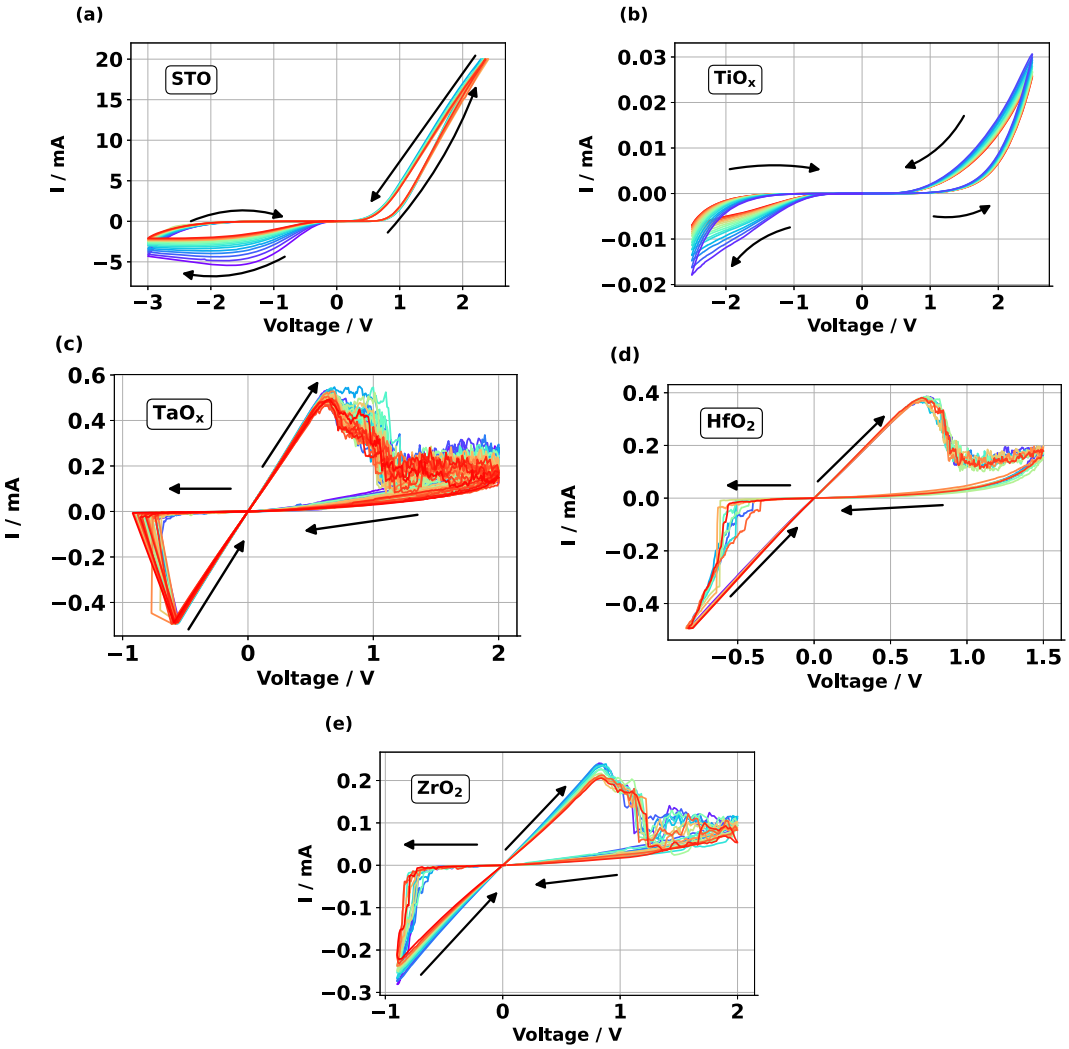

FIG. 4. Switching curves of STO (a), TiO_x (b), TaO_x (c), HfO_2 (d), and ZrO_x (e) devices. The switching direction is indicated by the arrows added to the plot. All sweeps were measured with a sweep rate of 1 V/s.

While pre-processing, the trace is split into a deterministic and a noise part. The different parts of an STO trace are shown in Fig. 3(c). In some traces, an oscillation with the frequency of the European power grid (50 Hz) was present. This was removed from the signal. For type 1 traces, we found a deterministic, fully volatile, saturation-like trend. The physical reason for this trend is under debate. This phenomenon is very similar to the short-term plasticity (STP) and might be an interesting property to make use of in the field of neuromorphic computing. As we see this drift as a deterministic and possibly beneficial part of the signal, we do not consider it as noise. We fitted the deterministic part by

$$I_{\mathrm{det}}(t) = A - B\,\exp(-\alpha \cdot t) + \beta \cdot t. \tag{1}$$

Thus, the noise signal is yielded

$$I_{\mathrm{noise}}(t) = I_{\mathrm{read}}(t) - I_{\mathrm{det}}(t). \tag{2}$$

For STO, note that the parameter A being in the range of 0.5–5 μA basically is the maximum or minimum of the trace. B is smaller than 1 μA, corresponding to the difference between the trace's maximum and minimum. Depending on the polarity of the read voltage, the sign of B changes. The main fitting parameters are the exponent α and the slope d. Here, α is between 2 s^{-1} and 10 s^{-1}, and β is smaller than 0.3 μA s^{-1}. For the TiO_x data, the parameters A, B, and β are in the range of the respective traces, whereas α is comparable. The average coefficient of determination is about $R^2 = 0.98$ for both the TiO_x and STO traces. For the type 2 devices, the read noise is defined as

$$I_{\mathrm{noise}}(t) = I_{\mathrm{read}}(t) - \mu(I_{\mathrm{read}}(t)), \tag{3}$$

as no systematic state drift was observed. Here, μ is the median of the trace.

IV. RESULTS

In this part, we first check, if the assignment of the material systems to the conduction types is correct. For this purpose, we use the I–V characteristic of the devices. Next, we analyze the worst-case and average signal-to-noise ratio (SNR) to quantify the amplitude of the read noise and calculate for every material system the cumulative distribution function (CDF) of the noise signal after filtering. This analysis gives an impression of the reliability of information stored after repeated reading. These quantities are highly sensitive to ionic noise. We also illustrate the structure of the read noise by showing representative traces for everyz material system.

First, we compare the switching curves seen in Figs. 4(a)–4(e) of the devices used in this paper with the switching characteristics expected for type 1 and 2 materials. Note that the voltage is defined with reference to 0 V at the active electrode. Here, all devices were in the HRS before sweeping. The switching direction is indicated by black arrows. Note that the STO and TiO_x devices are switched eightwise whereas the other devices are switched counter-eightwise.

The rather exponential I–V characteristic of the TiO_x and STO devices seen in Figs. 4(a) and 4(b) indicates that here a type 1 conduction mechanism can be assumed. The HfO_2, TaO_x, and ZrO_x [Figs. 4(c)–4(e)] sweeps exhibit comparably less exponential characteristics before switching occurs, as predicted for type 2 devices. The characteristics coincide with the predictions based on the band structure of the switching layer shown in Fig. 2(b).

We proceed by evaluating the read noise of the devices, checking if differences can be found between the two conduction types. For the sake of comparability, we normalize the traces by

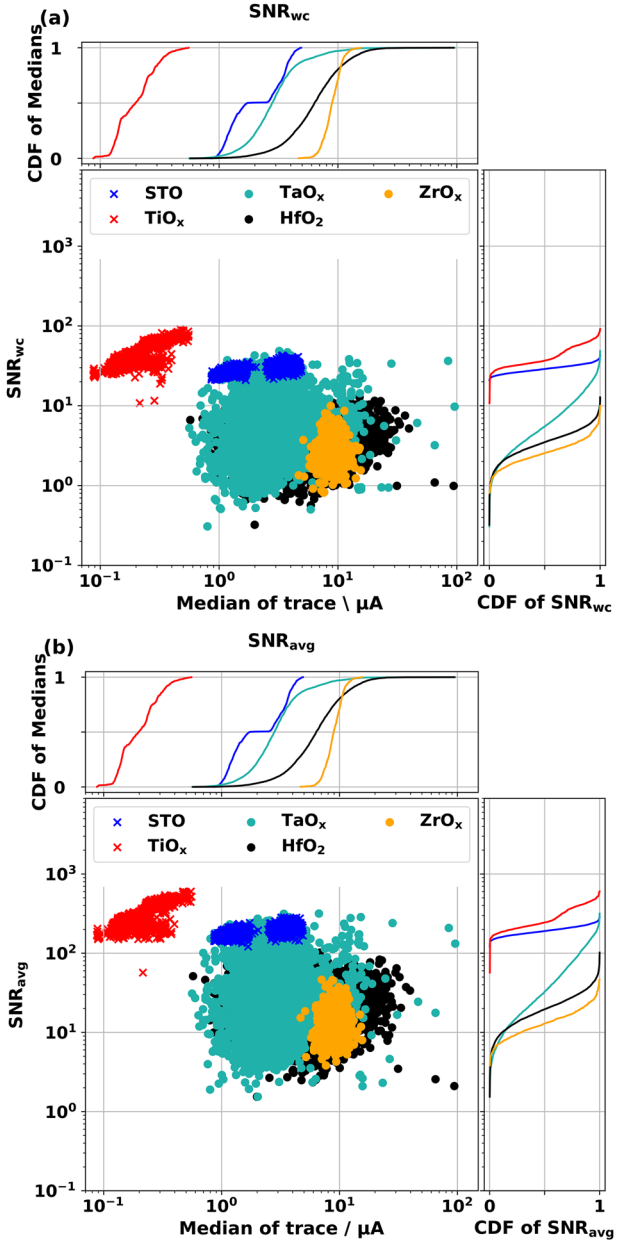

FIG. 5. (a) SNR_{wc} and (b) SNR_{avg} of the read noise traces taken for the different material systems. For type 1 materials, we see high SNR_{avg} values, making the definition of multiple states possible. For type 2 devices, the ionic noise behavior leads to a high level of noise.

$$\bar{I}_{\mathrm{noise}}(t) = \frac{I_{\mathrm{noise}}(t)}{\mu(I_{\mathrm{read}})} + 1, \tag{4}$$

where $I_{\mathrm{read}}(t)$ indicates the read current.

Three exemplary traces for each material system are shown in Fig. 6(a). The type 1 traces are dominated by the deterministic trend defined in Eq. (1), and no abrupt current jumps of measurable amplitude are seen. For type 2 traces, random current jumps of more than 8 μA are observed for all type 2 materials. This indicates noise induced by the reconfiguration of defects in the switching oxide.[39,40] Hence, for type 2 traces, the dominant source of noise is ionic noise. At the same time no deterministic trend is seen.

We use two parameters for the estimation of the relative amplitude of the noise signal: First,

$$\mathrm{SNR}_{\mathrm{wc}} = \frac{\mu(I_{\mathrm{read}})}{\max\limits_{t\in[0\,\mathrm{s},2\,\mathrm{s}]}(I_{\mathrm{noise}}(t)) - \min\limits_{t\in[0\,\mathrm{s},2\,\mathrm{s}]}(I_{\mathrm{noise}}(t))}, \tag{5}$$

as a worst-case error measure and, second,

$$\mathrm{SNR}_{\mathrm{avg}} = \frac{\mu(I_{\mathrm{read}})}{\sigma(I_{\mathrm{noise}})}, \tag{6}$$

as an average-case measure. Here, σ is the standard deviation.

The worst-case and average-case SNRs of the traces are shown in Figs. 5(a) and 5(b), respectively. It can be seen that the SNR of type 1 devices is in a well-defined range. Here, for STO traces, the minimum $\mathrm{SNR}_{\mathrm{wc}}$ is higher than 10 and $\mathrm{SNR}_{\mathrm{avg}}$ above 70. The STO data are split into two clusters, because of device to device variability. For TiO_x, the median of the read current is smaller, in accordance with the smaller area of the device. The smallest $\mathrm{SNR}_{\mathrm{wc}}$ values of the TiO_x traces are also higher than 10, even though the traces are a bit less uniform than for the STO devices.

For type 2 devices, a substantially larger spread of the SNR is observed. In the worst-case analysis, even noise amplitudes well above the median of the traces are seen over a wide range of resistive states. This is the case, if $\mathrm{SNR}_{\mathrm{wc}}$ is smaller than 1. Here, the best $\mathrm{SNR}_{\mathrm{wc}}$ is comparable to the worst values seen for STO. Comparing the type 2 material systems to each other, we see that the median TaO_x trace exhibits higher SNR values than the HfO_2 and ZrO_x traces. In particular, for the worst-case analysis, the biggest $\mathrm{SNR}_{\mathrm{wc}}$ of the TaO_x devices is almost one order of magnitude better than the best ZrO_x traces and is even better than those observed for STO devices. The reason is that, for TaO_x, traces

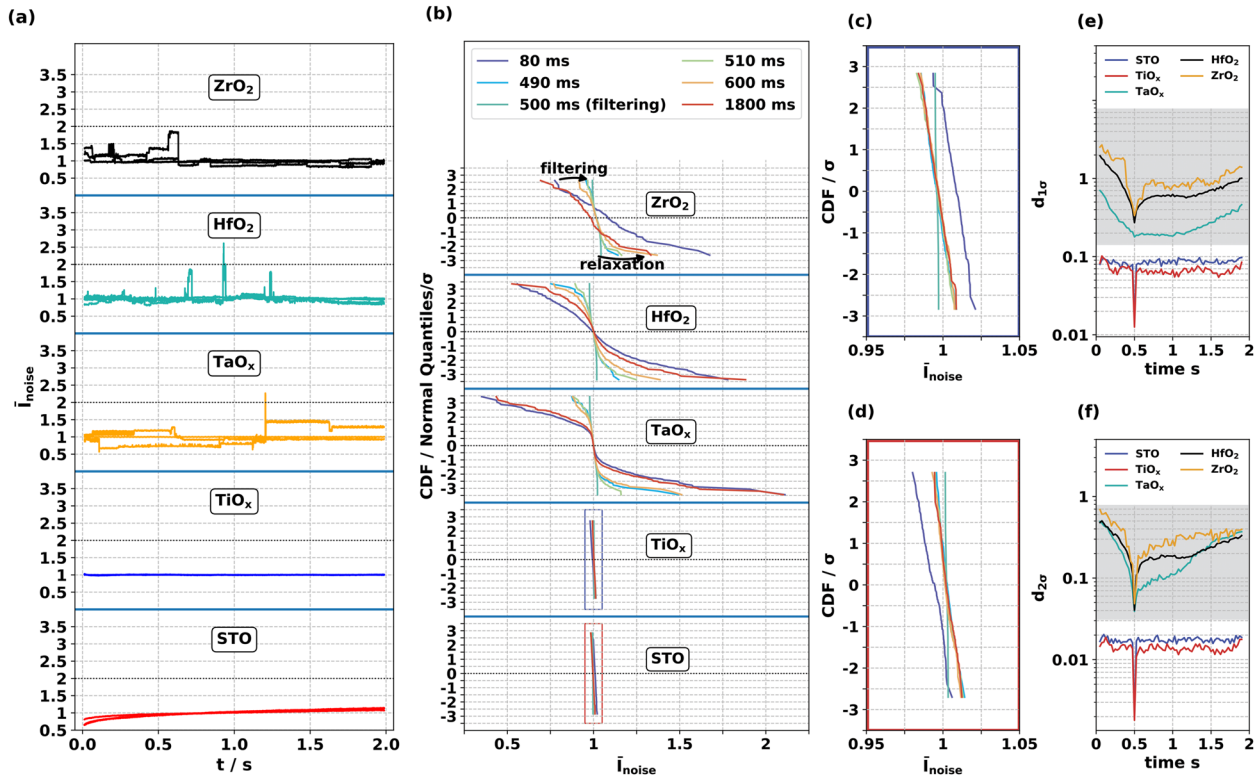

FIG. 6. (a) Three read noise traces with different noise amplitudes of each material system. We stress the ionic noise in the type 2 materials. (b) The CDF of the normalized read current at different times after the beginning of the read pulse. For this purpose, we filter traces within 0.5 σ around the median of $\bar{I}_{\mathrm{noise}}$ 500 ms after the start of the read pulse. For these read noise traces, the CDF at different time steps is shown. We see that for type 2 devices, the resistive state gradually widens up again after filtering, whereas for type 1 devices, no long-lasting effect of the filtering is seen. The type 1 data stays inside a narrow range. For ZrO_x a general drift towards lower read currents is seen. The CDF of TiO_x (c) and STO (d) are shown on a smaller scale. In (e) and (f), the range of the 1σ and 2σ surrounding, depending on the time after the beginning of the pulse, is plotted.

practically without ionic noise were observed. If ionic noise is observed, the amplitude can very well be in the range seen for the ZrO_x and HfO_2 traces.

To illustrate the intrinsic variability of the programmed states, we further analyze the stability of the traces by filtering all traces that are in a $\frac{\sigma}{2}$ surrounding of the median of $\bar{I}(t)$ at $t = 0.5$ s. From these traces, we calculate the CDF of $\bar{I}(t)$ at certain time steps before and after the filtering. The results of this analysis can be found in Fig. 6(b). Figures 6(c) and 6(d) show the CDF for STO and TiO_x on a smaller scale. The two conduction types show clearly different behavior. While the type 1 CDF stays similar at all time steps taken into account, the CDFs of the type 2 data start to relax into an intrinsic distribution after filtering. Especially for the TaO_x data, the distribution at the end of the measurement relaxed back into the state at the beginning. This relaxation limits the effectiveness of program verify algorithms.[24,39] The resulting width of the distribution must be taken into account if multiple states are to be programmed into a memory device.

We further investigate the kinetics of the relaxation by determining the range of the 1σ and 2σ surrounding

$$d_{n\sigma}(t) = |F_t^{-1}(y = \Phi(n)) - F_t^{-1}(y = \Phi(-n))|, \qquad n = 1, 2, \quad (7)$$

of the filtered data every 0.1 s. Here, F_t^{-1} is the inverse function of the CDF determined from the normalized noise at the time t, and Φ is the CDF of a normal distribution with mean and variance of 1. If F is a normal distribution, this yields

$$d_{n\sigma}(t) = \mu + n \cdot \sigma - (\mu - n \cdot \sigma) = 2n \cdot \sigma,$$

with 68% and 95% of the data being inside the border of this interval. In Figs. 6(e) and 6(f), $d_{1\sigma}(t)$ and $d_{2\sigma}(t)$ are shown, respectively. Here, the ranges for $d_{1\sigma}(t)$ and $d_{2\sigma}(t)$ are depending on the time. It can be seen that $d_{n\sigma}(t)$ of type 1 materials is substantially smaller than that for type 2 materials. Only when the traces are filtered we can see a dip in the range for type 1 devices. Hence, for the type 1 data, the relaxation into the relatively narrow distribution of $\bar{I}_{\text{noise}}$ is comparably faster. No big changes of the $d_{n\sigma}$ can be observed in the course of the measurement. Here, the main sources of noise are expected to be, e.g., environmental noise, while ionic noise would have a low amplitude because hopping between defect states is not the current limiting mechanism in type 1 materials; so single jumps cannot be detected.

For type 2 materials, the filtering has a longer lasting effect on $d_{n\sigma}$. This correlates with the fact that here the read noise is dominated by single ionic noise events. In case a jump was observed in only a small portion of the traces, $d_{1\sigma}$ stays constant. We again observe that for TaO_x, $d_{1\sigma}$ is smaller and that the relaxation is slower for both $d_{1\sigma}$ and $d_{2\sigma}$. This indicates that the mean time between two ionic noise events of TaO_x traces is substantially longer. The amplitude of the current jumps in TaO_x, if they are observed, is similar to those of HfO_2 and ZrO_x traces. $d_{2\sigma}$ of TaO_x and HfO_2 are similar, 0.8 s after the filtering. The relaxation is faster for the ZrO_x devices. This might be a result of the different energy barriers for the diffusion of the oxygen defects $V_O^{\bullet}$ seen in the switching oxides.

V. DISCUSSION

In short, our results are in good agreement with the theoretical predictions made based on DFT studies.[20,31,33] First, the I–V characteristics of the devices under test show typical band conduction and trap assisted tunneling behavior according to the material stacks. Second, there is a correlation between the SNR level and the type of the device. Third, the read noise could be analyzed semi-quantitatively.

Type 2 materials show a significantly reduced SNR for both the worst-case and average case analyses due to the occurrence of ionic noise. Thus, the ionic noise is a fingerprint of the type 2 conduction mechanism. For all type 2 materials, the maximum spread of the CDF, after filtering, was greater than 60% of the median of the trace. The frequency and average amplitude of ionic noise differ for the material systems under investigation. Here, single defects have a much higher impact on the total current compared to conduction type 1. For type 1 devices, the spread of the CDF seen in Fig. 6(b) stays smaller than 5% of the median of the trace.

We proved the need to distinguish ReRAM devices according to the conduction types as proposed by Funck and Menzel.[31] We infer that our results yield valuable information to optimally match material system and application. Based on our data, type 1 devices can best be used for memory tasks. A drawback here is the low switching speed of the TiO_x[30] and STO[52] devices in the switching mode used in this study. Type 2 devices exhibit favorable noise properties to be utilized, e.g., for probabilistic computing or noise generation in optimization tasks.

Nevertheless, we want to stress some challenges faced in this study. First, the exact band structure is depending not only on the material used, but also on the stoichiometry. During the forming process, the stoichiometry of the material under test can change.[53,54] This can lead to two different switching regimes that can be realized using the same devices.[20,51] Here, the dominating conduction mechanism can potentially change. Second, choosing the read voltage always is a compromise between, e.g., on–off ratio and read noise. Yet, the read voltages preferred by other authors can differ from this choice.[3,40,55,56]

VI. CONCLUSIONS

We measured two material systems based on type 1 and three stacks based on type 2 switching layers. This assignment is confirmed by the I–V characteristic of the respective devices. A clear correlation between the conduction mechanism and the read noise characteristics is demonstrated. We saw no ionic noise larger than the available measurement resolution for type 1 devices. This causes high SNR values. For type 2 devices, we saw ionic noise and low SNR values, partially smaller than 1.

Filtering the traces at a specific time after the beginning of the pulse has no long-lasting effect on type 1 devices. For type 2 material systems, ionic noise occurs in highly different rates, leading to different velocities of the CDF to widen up after filtering. This indicates that from the point of view of this study, type 1 material systems are a good match for data storage applications where read noise

should be avoided. Type 2 materials might be best fitting for probabilistic computing tasks or as a noise source to prevent overfitting in AI applications. As the event rate of ionic noise differs for the type 2 material systems, the frequency of occurrence can be chosen according to the respective application. Other properties can indicate otherwise.

Based on our results, tuning of the read noise characteristics should be enabled by the material design.

ACKNOWLEDGMENTS

We acknowledge the DFG (German Science Foundation) for funding our work within the framework of the collaborative research center SFB 917 "Nanoswitches." Moreover, we emphasize our acknowledgment for the additional funding provided by the Helmholtz Association Initiative and Networking Fund under Project No. SO-092 (Advanced Computing Architectures, ACA) and the Federal Ministry of Education and Research (BMBF, Germany) in the project NEUROTEC (Project Nos. 16ME0398K and 16ME0399) and NeuroSys (Project No. 03ZU1106AB).

Of all our colleagues with whom we had fruitful discussions, we want to highlight Moritz von Witzleben, Xiaohua Liu, Thomas Heisig, and Alexander Gutsche. We especially thank Professor Rainer Waser for the support for this work.

AUTHOR DECLARATIONS

Conflict of Interest

The authors have no conflicts to disclose.

Author Contributions

K. Schnieders: Data curation (equal); Investigation (equal); Software (equal); Visualization (equal). **C. Funck**: Conceptualization (equal); Methodology (equal). **F. Cüppers**: Resources (equal). **S. Aussen**: Resources (equal). **T. Kempen**: Resources (equal). **A. Sarantopoulos**: Resources (equal). **R. Dittmann**: Conceptualization (equal); Resources (equal); Validation (equal). **S. Menzel**: Conceptualization (equal); Validation (equal). **V. Rana**: Resources (equal). **S. Hoffmann-Eifert**: Conceptualization (equal); Resources (equal); Validation (equal). **S. Wiefels**: Conceptualization (equal); Supervision (equal); Validation (equal).

DATA AVAILABILITY

The data that support the findings of this study are available from the corresponding author upon reasonable request.

REFERENCES

[1] H.-Y. Chen, S. Yu, B. Gao, P. Huang, J. Kang, and H.-S. P. Wong, "HfOx based vertical resistive random access memory for cost-effective 3D cross-point architecture without cell selector," in *2012 IEEE International Electron Devices Meeting (IEDM)* (IEEE, 2012).

[2] Q. Luo, X. Xu, T. Gong, H. Lv, D. Dong, H. Ma, P. Yuan, J. Gao, J. Liu, Z. Yu, J. Li, S. Long, Q. Liu, and M. Liu, "8-Layers 3D vertical RRAM with excellent scalability towards storage class memory applications," in *2017 IEEE International Electron Devices Meeting (IEDM)* (IEEE, 2017).

[3] T. Kempen, R. Waser, and V. Rana, "50x Endurance improvement in TaOx RRAM by extrinsic doping," in *2021 IEEE International Memory Workshop (IMW)* (IEEE, 2021).

[4] J. J. Yang, M. Zhang, J. P. Strachan, F. Miao, M. D. Pickett, R. D. Kelley, G. Medeiros-Ribeiro, and R. S. Williams, "High switching endurance in TaO_x memristive devices," Appl. Phys. Lett. **97**, 232102 (2010).

[5] S. Goswami, A. J. Matula, S. P. Rath, S. Hedstrom, S. Saha, M. Annamalai, D. Sengupta, A. Patra, S. Ghosh, H. Jani, S. Sarkar, M. R. Motapothula, C. A. Nijhuis, J. Martin, S. Goswami, V. S. Batista, and T. Venkatesan, "Robust resistive memory devices using solution-processable metal-coordinated azo aromatics," Nat. Mater. **16**, 1216 (2017).

[6] H. Jiang, L. Han, P. Lin, Z. Wang, M. H. Jang, Q. Wu, M. Barnell, J. J. Yang, H. L. Xin, and Q. Xia, "Sub-10 nm Ta channel responsible for superior performance of a HfO_2 memristor," Sci. Rep. **6**, 28525 (2016).

[7] S. Wiefels, U. Böttger, S. Menzel, D. J. Wouters, and R. Waser, "Statistical modeling and understanding of HRS retention in 2.5 Mb HfO_2 based ReRAM," in *2020 IEEE International Memory Workshop (IMW)* (IEEE, 2020).

[8] S. Wiefels, U. Böttger, S. Menzel, D. J. Wouters, and R. Waser, "Empirical tunneling model describing the retention of 2.5 Mb HfO_2 based ReRAM," in *International Symposium On VLSI Technology, Systems and Application (VLSI-TSA)* (IEEE, 2020).

[9] M. von Witzleben, T. Hennen, A. Kindsmüller, S. Menzel, R. Waser, and U. Böttger, "Study of the SET switching event of VCM-based memories on a picosecond timescale," J. Appl. Phys. **127**, 204501 (2020).

[10] M. von Witzleben, S. Wiefels, A. Kindsmüller, P. Stasner, F. Berg, F. Cüppers, S. Hoffmann-Eifert, R. Waser, S. Menzel, and U. Böttger, "Intrinsic RESET speed limit of valence change memories," ACS Appl. Electron. Mater. **3**, 5563–5572 (2021).

[11] Z. Wang, H. Wu, G. W. Burr, C. S. Hwang, K. L. Wang, Q. Xia, and J. J. Yang, "Resistive switching materials for information processing," Nat. Rev. Mater. **5**, 173–195 (2020).

[12] R. Waser, R. Dittmann, S. Menzel, and T. Noll, "Introduction to new memory paradigms: Memristive phenomena and neuromorphic applications," Faraday Discuss. **213**, 11–27 (2019).

[13] S. Stathopoulos, A. Khiat, M. Trapatseli, S. Cortese, A. Serb, I. Valov, and T. Prodromakis, "Multibit memory operation of metal-oxide bi-layer memristors," Sci. Rep. **7**, 17532 (2017).

[14] D. Bhattacharjee, R. Devadoss, and A. Chattopadhyay, "ReVAMP: ReRAM based VLIW architecture for in-memory computing," in *Design, Automation and Test in Europe Conference and Exhibition (DATE) 2017* (IEEE, 2017).

[15] D. Bhattacharjee, W. Kim, A. Chattopadhyay, R. Waser, and V. Rana, "Multivalued and fuzzy logic realization using TaOx memristive devices," Sci. Rep. **8**, 8–10 (2018).

[16] P. Chi, S. Li, C. Xu, T. Zhang, J. Zhao, Y. Liu, Y. Wang, and Y. Xie, "Prime: A novel processing-in-memory architecture for neural network computation in ReRAM-based main memory," in *2016 ACM/IEEE 43rd Annual International Symposium on Computer Architecture (ISCA)* (IEEE, 2016).

[17] G. W. Burr, R. M. Shelby, A. Sebastian, S. Kim, S. Kim, S. Sidler, K. Virwani, M. Ishii, P. Narayanan, A. Fumarola, L. L. Sanches, I. Boybat, M. Le Gallo, K. Moon, J. Woo, H. Hwang, and Y. Leblebici, "Neuromorphic computing using non-volatile memory," Adv. Phys.: X **2**, 89–124 (2017).

[18] A. Sood, A. D. Poletayev, D. A. Cogswell, P. M. Csernica, J. T. Mefford, D. Fraggedakis, M. F. Toney, A. M. Lindenberg, M. Z. Bazant, and W. C. Chueh, "Electrochemical ion insertion from the atomic to the device scale," Nat. Rev. Mater. **6**, 847–867 (2021).

[19] E. Lim and R. Ismail, "Conduction mechanism of valence change resistive switching memory: Survey," Electronics **4**, 586–613 (2015).

[20] H. Zhang, S. Yoo, S. Menzel, C. Funck, F. Cüppers, D. J. Wouters, C. S. Hwang, R. Waser, and S. Hoffmann-Eifert, "Understanding the coexistence of two bipolar resistive switching modes with opposite polarity in $Pt/TiO_2/Ti/Pt$ nanosized ReRAM devices," ACS Appl. Mater. Interfaces **10**, 29766–29778 (2018).

[21] C. Kügeler, J. Zhang, S. Hoffmann-Eifert, S. K. Kim, and R. Waser, "Nanostructured resistive memory cells based on 8-nm-thin TiO_2 films deposited

by atomic layer deposition," J. Vac. Sci. Technol., B: Nanotechnol. Microelectron.: Mater., Process., Meas., Phenom. **29**, 01AD01 (2011).
[22]H. Zhang, N. Aslam, M. Reiners, R. Waser, and S. Hoffmann-Eifert, "Atomic layer deposition of TiO_x/Al_2O_3 bilayer structures for resistive switching memory applications," Chem. Vap. Deposition **20**, 282–290 (2014).
[23]R. B. Jacobs-Gedrim, S. Agarwal, R. S. Goeke, C. Smith, P. S. Finnegan, J. Niroula, D. R. Hughart, P. G. Kotula, C. D. James, and M. J. Marinella, "Analog high resistance bilayer RRAM device for hardware acceleration of neuromorphic computation," J. Appl. Phys. **124**, 202101 (2018).
[24]A. Fantini, G. Gorine, R. Degraeve, L. Goux, C. Chen, A. Redolfi, S. Clima, A. Cabrini, G. Torelli, and M. Jurczak, "Intrinsic program instability in HfO_2 RRAM and consequences on program algorithms," in *Electron Devices Meeting (IEDM), 2015 IEEE International* (IEEE, 2015).
[25]E. Abbaspour, S. Menzel, and C. Jungemann, "Random telegraph noise analysis in redox-based resistive switching devices using KMC simulations," in *2017 International Conference on Simulation of Semiconductor Processes and Devices (SISPAD), September 7–9* (IEEE, Kamakura, Japan, 2017).
[26]P. Huang, D. B. Zhu, C. Liu, Z. Zhou, Z. Dong, H. Jiang, W. S. Shen, L. F. Liu, X. Y. Liu, and J. F. Kang, "RTN based oxygen vacancy probing method for Ox-RRAM reliability characterization and its application in tail bits," in *2017 IEEE International Electron Devices Meeting (IEDM)* (IEEE, 2017).
[27]F.-C. Chang, Y.-H. Huang, C.-J. Lin, and Y.-C. King, "A study of read variability in backfill contact random access memory," in *International Symposium on VLSI Technology, Systems and Application (VLSI-TSA)* (IEEE, Hsinchu, Taiwan, 2020).
[28]E. O. Neftci, B. U. Pedroni, S. Joshi, M. Al-Shedivat, and G. Cauwenberghs, "Stochastic synapses enable efficient brain-inspired learning machines," Front. Neurosci. **10**, 241 (2016).
[29]G. Indiveri, B. Linares-Barranco, R. Legenstein, G. Deligeorgis, and T. Prodromakis, "Integration of nanoscale memristor synapses in neuromorphic computing architectures," Nanotechnology **24**, 384010 (2013).
[30]W. Wang, B. Hoffer, T. Greenberg-Toledo, Y. Li, M. Zou, E. Herbelin, R. Ronen, X. Xu, Y. Zhao, J. Yang, and S. Kvatinsky, "Efficient training of the memristive deep belief net immune to non-idealities of the synaptic devices," Adv. Intell. Syst. **4**, 2100249 (2022).
[31]C. Funck and S. Menzel, "Comprehensive model of electron conduction in oxide-based memristive devices," ACS Appl. Electron. **3**, 3674–3692 (2021).
[32]C. Linderälv, A. Lindman, and P. Erhart, "A unifying perspective on oxygen vacancies in wide band gap oxides," J. Phys. Chem. Lett. **9**, 222–228 (2018).
[33]C. Funck, A. Marchewka, C. Bäumer, P. C. Schmidt, P. Müller, R. Dittmann, M. Martin, R. Waser, and S. Menzel, "A theoretical and experimental view on the temperature dependence of the electronic conduction through a Schottky barrier in a resistively switching $SrTiO_3$-based memory cell," Adv. Electron. Mater. **4**, 1800062 (2018).
[34]C. Funck, C. Bäumer, S. Wiefels, T. Hennen, R. Waser, S. Hoffmann-Eifert, R. Dittmann, and S. Menzel, "Comprehensive model for the electronic transport in $Pt/SrTiO_3$ analog memristive devices," Phys. Rev. B **102**, 035307 (2020).
[35]C. M. M. Rosário, B. Thöner, A. Schönhals, S. Menzel, M. Wuttig, R. Waser, N. A. Sobolev, and D. J. Wouters, "Correlation between the transport mechanisms in conductive filaments inside Ta_2O_5-based resistive switching devices and in substoichiometric TaO_x thin films," Appl. Phys. Lett. **112**, 213504 (2018).
[36]F. M. Puglisi, L. Larcher, A. Padovani, and P. Pavan, "A complete statistical investigation of RTN in HfO_2-based RRAM in high resistive state," IEEE Trans. Electron Devices **62**, 2606–2613 (2015).
[37]S. Ambrogio, S. Balatti, A. Cubeta, A. Calderoni, N. Ramaswamy, and D. Ielmini, "Understanding switching variability and random telegraph noise in resistive RAM," in *2013 IEEE International Electron Devices Meeting (IEDM)* (IEEE, 2013).
[38]M. Terai, Y. Sakotsubo, Y. Saito, S. Kotsuji, and H. Hada, "Memory-state dependence of random telegraph noise of Ta_2O_5/TiO_2 stack ReRAM," IEEE Electron Device Lett. **31**, 1302–1304 (2010).
[39]S. Wiefels, C. Bengel, N. Kopperberg, K. Zhang, R. Waser, and S. Menzel, "HRS instability in oxide based bipolar resistive switching cells," IEEE Trans. Electron Devices **67**, 4208–4215 (2020).
[40]N. Kopperberg, S. Wiefels, S. Liberda, R. Waser, and S. Menzel, "A consistent model for short-term instability and long-term retention in filamentary oxide-based memristive devices," ACS Appl. Mater. Interfaces **13**, 58066–58075 (2021).
[41]J. Bernamont, "Fluctuations in the resistance of thin films," Proc. Phys. Soc. **49**, 138–139 (1937).
[42]J. P. Campbell, J. Qin, K. P. Cheungl, L. Yu, J. S. Suehle, A. Oates, and K. Sheng, "The origins of random telegraph noise in highly scaled SiON nMOSFETs," in *2008 IEEE International Integrated Reliability Workshop Final Report, 2008 IEEE International Integrated Reliability Workshop Final Report* (IEEE, 2008).
[43]S. Lee, H.-J. Cho, Y. Son, D. S. Lee, and H. Shin, "Characterization of oxide traps leading to RTN in high-k and metal gate MOSFETs," in *2009 IEEE International Electron Devices Meeting (IEDM), 2009 IEEE International Electron Devices Meeting (IEDM)* (IEEE, 2009).
[44]K.-H. Yang, T.-Y. Chen, N.-J. Ho, and H.-Y. Lu, "In-gap states in wide-band-gap $SrTiO_3$ analyzed by cathodoluminescence," J. Am. Ceram. Soc. **94**, 1811–1816 (2011).
[45]P. Reckers, M. Dimamay, J. Klett, S. Trost, K. Zilberberg, T. Riedl, B. A. Parkinson, J. Brötz, W. Jaegermann, and T. Mayer, "Deep and shallow TiO_2 gap states on cleaved anatase single crystal (101) surfaces, nanocrystalline anatase films, and ALD titania ante and post annealing," J. Phys. Chem. C **119**, 9890–9898 (2015).
[46]V. A. Gritsenko, T. V. Perevalov, V. A. Voronkovskii, A. A. Gismatulin, V. N. Kruchinin, V. S. Aliev, V. A. Pustovarov, I. P. Prosvirin, and Y. Roizin, "Charge transport and the nature of traps in oxygen deficient tantalum oxide," ACS Appl. Mater. Interfaces **10**, 3769–3775 (2018).
[47]H. Takeuchi, D. Ha, and T.-J. King, "Observation of bulk HfO_2 defects by spectroscopic ellipsometry," J. Vac. Sci. Technol., A **22**, 1337–1341 (2004).
[48]A. Kumar, S. Mondal, and K. S. R. Koteswara Rao, "Experimental evidences of charge transition levels in ZrO_2 and at the Si: ZrO_2 interface by deep level transient spectroscopy," Appl. Phys. Lett. **110**, 132904 (2017).
[49]A. Hardtdegen, C. La Torre, F. Cüppers, S. Menzel, R. Waser, and S. Hoffmann-Eifert, "Improved switching stability and the effect of an internal series resistor in HfO_2/TiO_x bilayer ReRAM cells," IEEE Trans. Electron Devices **65**, 3229–3236 (2018).
[50]J. L. Rieck, F. V. E. Hensling, and R. Dittmann, "Trade-off between variability and retention of memristive epitaxial $SrTiO_3$ devices," APL Mater. **9**, 021110 (2021).
[51]S. Aussen, F. Cüppers, R. Waser, and S. Hoffmann-Eifert, "Direct comparison of the SET kinetics of a TiO_x/Al_2O_3-based memristive cell in filamentary- and area-mode," in *2022 IEEE 22st International Conference on Nanotechnology (NANO)* (IEEE, 2022).
[52]S. Siegel, C. Baeumer, A. Gutsche, M. Witzleben, R. Waser, S. Menzel, and R. Dittmann, "Trade-off between data retention and switching speed in resistive switching ReRAM devices," Adv. Electron. Mater. **7**, 2000815 (2020).
[53]J. P. Strachan, M. D. Pickett, J. J. Yang, S. Aloni, A. L. D. Kilcoyne, G. Medeiros-Ribeiro, and R. S. Williams, "Direct identification of the conducting channels in a functioning memristive device," Adv. Mater. **22**, 3573–3577 (2010).
[54]J. P. Strachan, D. B. Strukov, J. Borghetti, J. J. Yang, G. Medeiros-Ribeiro, and R. Stanley Williams, "The switching location of a bipolar memristor: Chemical, thermal and structural mapping," Nanotechnology **22**, 254015 (2011).
[55]C. Bengel, F. Cüppers, M. Payvand, R. Dittmann, R. Waser, S. Hoffmann-Eifert, and S. Menzel, "Utilizing the switching stochasticity of HfO_2/TiO_x-based ReRAM devices and the concept of multiple device synapses for the classification of overlapping and noisy patterns," Front. Neurosci. **15**, 621 (2021).
[56]T. Heisig, J. Kler, H. Du, C. Baeumer, F. Hensling, M. Glöß, M. Moors, A. Locatelli, T. O. Mentes, and F. Genuzio, "Antiphase boundaries constitute fast cation diffusion paths in $SrTiO_3$ memristive devices," Adv. Funct. Mater. **30**, 2004118 (2020).